



A long noncoding RNA influences the choice of the X chromosome to be inactivated

Andreas Hierholzer^{a,1}, Corinne Chureau^b, Alessandra Liverziani^a, Nerea Blanes Ruiz^c, Bruce M. Cattanach^d, Alexander N. Young^{a,2}, Manish Kumar^{a,3}, Andrea Cerase^{a,4}, and Phil Avner^{a,5}

Edited by Robb Krumlauf, Stowers Institute for Medical Research, Kansas City, MO; received October 11, 2021; accepted April 23, 2022

X chromosome inactivation (XCI) is the process of silencing one of the X chromosomes in cells of the female mammal which ensures dosage compensation between the sexes. Although theoretically random in somatic tissues, the choice of which X chromosome is chosen to be inactivated can be biased in mice by genetic element(s) associated with the so-called X-controlling element (*Xce*). Although the *Xce* was first described and genetically localized nearly 40 y ago, its mode of action remains elusive. In the approach presented here, we identify a single long noncoding RNA (lncRNA) within the *Xce* locus, *Lppnx*, which may be the driving factor in the choice of which X chromosome will be inactivated in the developing female mouse embryo. Comparing weak and strong *Xce* alleles we show that *Lppnx* modulates the expression of *Xist lncRNA*, one of the key factors in XCI, by controlling the occupancy of pluripotency factors at Intron1 of *Xist*. This effect is counteracted by enhanced binding of Rex1 in *DxPas34*, another key element in XCI regulating the activity of Tsix lncRNA, the main antagonist of *Xist*, in the strong but not in the weak *Xce* allele. These results suggest that the different susceptibility for XCI observed in weak and strong *Xce* alleles results from differential transcription factor binding of *Xist* Intron 1 and *DxPas34*, and that *Lppnx* represents a decisive factor in explaining the action of the *Xce*.

X chromosome inactivation | X-controlling element | pluripotency factors | female mouse embryo | noncoding RNA

Many metazoa, when undergoing sex differentiation, adopt dosage compensation systems which through varied biological approaches, ensure the equalization of the transcription dosage of the sex chromosomes in the different sexes (1, 2). In flies, for example, hypertranscription of the X chromosome doubles the level of X chromosome transcriptional activity in males to achieve levels comparable to that ensured by the two X chromosomes present in females (3). In contrast, in mammals, inactivation of one of the two X chromosome present in females occurs, a process known as X chromosome inactivation (XCI) (4–7). In female mice, two forms of XCI exist. In imprinted XCI (iXCI) the exclusive inactivation of the male-derived X chromosome is observed as opposed to random XCI (rXCI), in which cells of the epiblast choose to inactivate either the male or female inherited X (8).

In mouse preimplantation embryos iXCI begins gradually at the two-cell stage and by the morula stage this process is complete, with each cell containing an inactivated and silenced paternal X chromosome. At the late blastocyst stage, this process is reversed within cells of the inner cell mass, which will give rise to the embryo proper, while cells from extraembryonal tissues such as the trophectoderm and primitive endoderm maintain the silencing of the paternal X.

This results at the time of implantation, in cells of the epiblast carrying two fully active X chromosomes. Between days 5.5 and 7.5 in their turn, cells of the epiblast undergo random XCI with the exact timepoint of XCI of each cell depending on the germ layer to which it belongs (9).

By day 9.5 the process of rXCI is essentially complete, with the female embryo consisting of a mosaic of cells carrying either paternal or maternal derived inactivated X chromosomes. This pattern persists in the soma throughout postnatal life as the cell passes on the X which has been inactivated to its daughter cells through mitosis. As the timepoint of rXCI in the early postimplantation embryo coincides with the formation of the three germ layers, it has been proposed that the rXCI process is tightly coupled to the process of differentiation (10). This notion is supported by studies on embryonic stem cells (ES) which have been exploited as an *in-vitro* model for the study of rXCI. In female pluripotent ES cells both X chromosomes are equally transcribed. Early in the *in vitro* differentiation the initiation of inactivation of a single X occurs in a random fashion (11).

At the molecular level, XCI in the mouse has been shown to be highly dependent on the expression of two long-noncoding RNAs (lncRNAs), *Xist* and its antisense

Significance

Long noncoding RNAs (lncRNA) play a fundamental role in the process of X-chromosome inactivation. Here we show that these kind of RNAs are also involved in the choice of which chromosome, paternal or maternal, is going to be inactivated in female mice. We identify the lncRNA *Lppnx* as the driving force for the action of the so-called X-controlling element (*Xce*). Although the *Xce* had been described 40 y ago, its localization on the X chromosome together with its molecular action remain elusive. With the results presented here, we shed light on the specific localization of the *Xce* as well as on the underlying molecular mechanisms how the *Xce* influences the choice of which chromosome is going to be inactivated.

Author contributions: A.H., C.C., A.C., and P.A. designed research; B.M.C., A.N.Y., and M.K. provided theoretical input to the project; A.H., C.C., A.L., and N.B.R. performed research; A.H. and C.C. contributed new reagents/analytic tools; A.H. and C.C. analyzed data; and A.H. and P.A. wrote the paper.

The authors declare no competing interest.

This article is a PNAS Direct Submission.

Copyright © 2022 the Author(s). Published by PNAS. This open access article is distributed under Creative Commons Attribution-NonCommercial-NoDerivatives License 4.0 (CC BY-NC-ND).

¹Present address: Department of Biosystems Science and Engineering, ETH Zürich, 4058 Basel, Switzerland.

²Present address: Blizard Institute, Barts and The London School of Medicine and Dentistry, Queen Mary University of London, London, E1 2AT, United Kingdom.

³Present address: Department of Neurosurgery, Medical College of Georgia, Augusta University, 30912 Augusta, GA

⁴Present address: Department of Biology, Università di Pisa, 56126 Pisa, Italy.

⁵To whom correspondence may be addressed. Email: philip.avner@embl.it.

This article contains supporting information online at <http://www.pnas.org/lookup/suppl/doi:10.1073/pnas.2118182119/-DCSupplemental>.

Published July 5, 2022.

counterpart *Tsix* (12, 13). While in undifferentiated cells *Xist* and *Tsix* are equally transcribed, at the onset of differentiation *Xist* is up-regulated and *Tsix* down-regulated from the same X chromosome. In the course of differentiation *Xist* starts to spread over the whole chromosome, attracting histone-modifying complexes like Polycomb repressive complex 1/2 (PRC1/2) and DNA methyltransferases, which will lead to the complete transcriptional silencing and the formation of a heterochromatic environment visible as the Barr body (14).

Genetically, *Xist/Tsix* localize to a region called the X inactivation center (XIC). This region, extending over roughly 500 kb, is both required and sufficient to drive XCI. The region contains additional lncRNAs such as *Ftx*, *Xite*, and *Jpx*, which modulate *Xist* or/and *Tsix* expression (15–17). Studies using ES cells have shown that pluripotency factors are involved in XCI, suggesting again the likelihood of tight and mechanistically meaningful coupling between differentiation and XCI. Part of the generic role of these factors involves the direct blocking of *Xist* and promotion of *Tsix* transcription, with the key pluripotency factors Oct4, Sox2, and Nanog having been shown to bind to Intron1 of *Xist* and block its transcription (18). Conversely, Rex1, Klf4, and c-myc bind to a minisatellite repeat, *DxPas34*, upstream of the *Tsix* gene to promote its transcription (19). While genetic deletion of *DxPas34* leads to ectopic up-regulation of *Xist*, overexpression of Rex1 inhibits *Xist* up-regulation and XCI. Rex1 plays a crucial role in the initiation and fine-tuning of XCI through its interaction with RNF12, an X-linked ubiquitin ligase which is up-regulated at the onset of differentiation and processes the proteasomal degradation of Rex1 (20). RNF12 is also controlled by other pluripotency factors (21).

The initiation of rXCI is thought to require the recognition of the X chromosome (counting) and the decision of which chromosome will be inactivated (choice). Although the choice of which X chromosome will be inactivated in somatic tissues is theoretically random, it has been shown that alleles of the X-controlling element (*Xce*) can significantly bias the ratio of inactivation between the Xs present in the female (22, 23). Four alleles have been identified among standard inbred mouse strains and inbred wild mouse, according to their behavior in various XCI crosses: *Xce^a* (129Sv, C3H, CBA), *Xce^b* (BALB/C, C57Bl6, DBA), *Xce^c* (Pgl1a, *Mus castaneus*) and *Xce^d* (*Mus spretus*) with allelic strength ranging from “weak, *Xce^a* < intermediate, *Xce^b* < strong, *Xce^c* < very strong, *Xce^d* (24–27). In mice, heterozygous for the *Xce*, the chromosome carrying the weaker allele is more likely to be inactivated, leading to the skewed XCI ratio. For example, 129Sv/Pgl1a heterozygous females show a 75:25 ratio, meaning that some 25% of the cells carry an inactivated Pgl1a-derived X chromosome while 75% of cells had inactivated the 129Sv-derived X (28). *Xce* homozygous animals, irrespective of the allele carried, do not exhibit such skewing (29).

Although the *Xce* was first described nearly four decades ago, the identity and precise genomic localization remains elusive. Initially, the *Xce* was located between *Eda* (*Tabby*) and *Atp7a* (*Mottled*), spanning roughly 9 Mb and encompassing the XIC with *Xist/Tsix* (30–32). That *Xist* is part of, or even identical to the *Xce* locus, was disproved several years later (33). Several more recent attempts have been undertaken to identify the genomic loci driving skewed XCI without answering the question whether one or several genomic loci are implicated (33–35).

Here we report a further approach to determine a possible candidate for the *Xce*. Analyzing previous mapping data which localized the *Xce* candidate region between *DxPas28* and *DxPas41* encompassing 80 kb and two protein coding genes (*Cdx4* and *Chic1*), we found a transcriptionally active locus which had gone unreported. Further experiments revealed that the resulting

transcript, which we named Lppnx, is mainly localized in the nucleus and that its expression is restricted to the inner cell mass (ICM) of blastocysts in male as well as in female ES cells. Deletion of the putative promoter region in ES cells and mice disrupts expression of Lppnx and does not affect pluripotency or viability. However, upon differentiation we detect elevated expression of *Xist* in female as well as in male cells compared to WT cells. In addition, when Lppnx-deficient 129Sv animals (weak *Xce*) were crossed with Pgl1a mice (strong *Xce*), we detected a shift toward expression of the strong allele of *Xist* as well as a shift in the allelic ratio of X-linked gene expression, indicating that Lppnx may act as a negative regulator of *Xist* and thus influence the choice of which X will be inactivated. By analyzing high-order chromatin (Hi-C) data, we established that the *Lppnx* locus interacts with *Xist* Intron1, an important regulator of *Xist* transcription. Deletion of *Xist* Intron1 in 129Sv Lppnx-deficient male ES cells rescues the expected *Xce* phenotype, indicating that Lppnx acts via *Xist* intron 1. In addition, ChIP experiments reveal that in Lppnx-deficient ES cells Oct4 and Rex1 occupancy of Intron1 is decreased, showing a possible regulatory network in which Lppnx modulates the occupancy of pluripotency factors at *Xist* Intron1 and hence, *Xist* transcription upon differentiation.

Results

Mapping of the *Xce* Candidate Region and Its Genetic Elements.

In a previous study (33) and subsequent follow-up studies, we identified a roughly 80 kb element 3' to *Xist* between the microsatellite repeats *DxPas28* and *41*, as a potential *Xce* candidate (Fig. 1A). In addition to the previously characterized protein coding genes *Cdx4* and *Chic1*, we identified another transcript originating from the candidate region (*SI Appendix, Fig. S1A*). Analysis of published ChIP-seq data of ES cells allowed us to identify a putative promoter region of 600 bp harboring binding sites for the pluripotency factors Oct4, Sox2, and Nanog as well as PolII, indicating active transcription (Fig. 1B). This is supported by the observation of H3K79me2 marks in the gene body, a consequence of active transcription (36).

A Long Noncoding RNA within the *Xce* Expressed in ES Cells and in the ICM of Blastocysts.

Using primers binding to the first exon of the unknown transcript, we analyzed various tissues and cell lines to elucidate its expression pattern. Apart from weak expression in ovary and brain, we did not find transcripts in adult mouse organs nor in male or female fibroblast cell lines, whereas male and female ES cells showed a robust signal (Fig. 1C). This indicates that expression of the transcript is likely restricted to undifferentiated stem cells. In line with this conclusion, using an RNA-fluorescent in situ hybridization (FISH) approach we found a comparable signal in the ICM of expanded blastocysts indicating expression in the mouse preimplantation embryos (*SI Appendix, Fig. S1B*). To address whether the transcript encodes a protein we fractionated ES cell extracts into nuclei and cytosolic fractions. We found the vast majority of transcripts in the nucleus, indicating a likely noncoding RNA (Fig. 1D). This result is supported by RNA-FISH experiments showing a clear signal in the nucleus of both male and female ES cells (Fig. 1E). Given its restricted expression to ES cells and the early embryo, we were interested to explore the eventual dependency of its expression on pluripotency factors. To this end we made use of an *Oct4*-deficient ES cell line which carries a tetracycline-repressible *Oct4* transgene (37). Differentiation of these ES cells in the presence of tetracycline (i.e., in the absence of Oct4) leads to a rapid down-regulation of the transcript, whereas in the

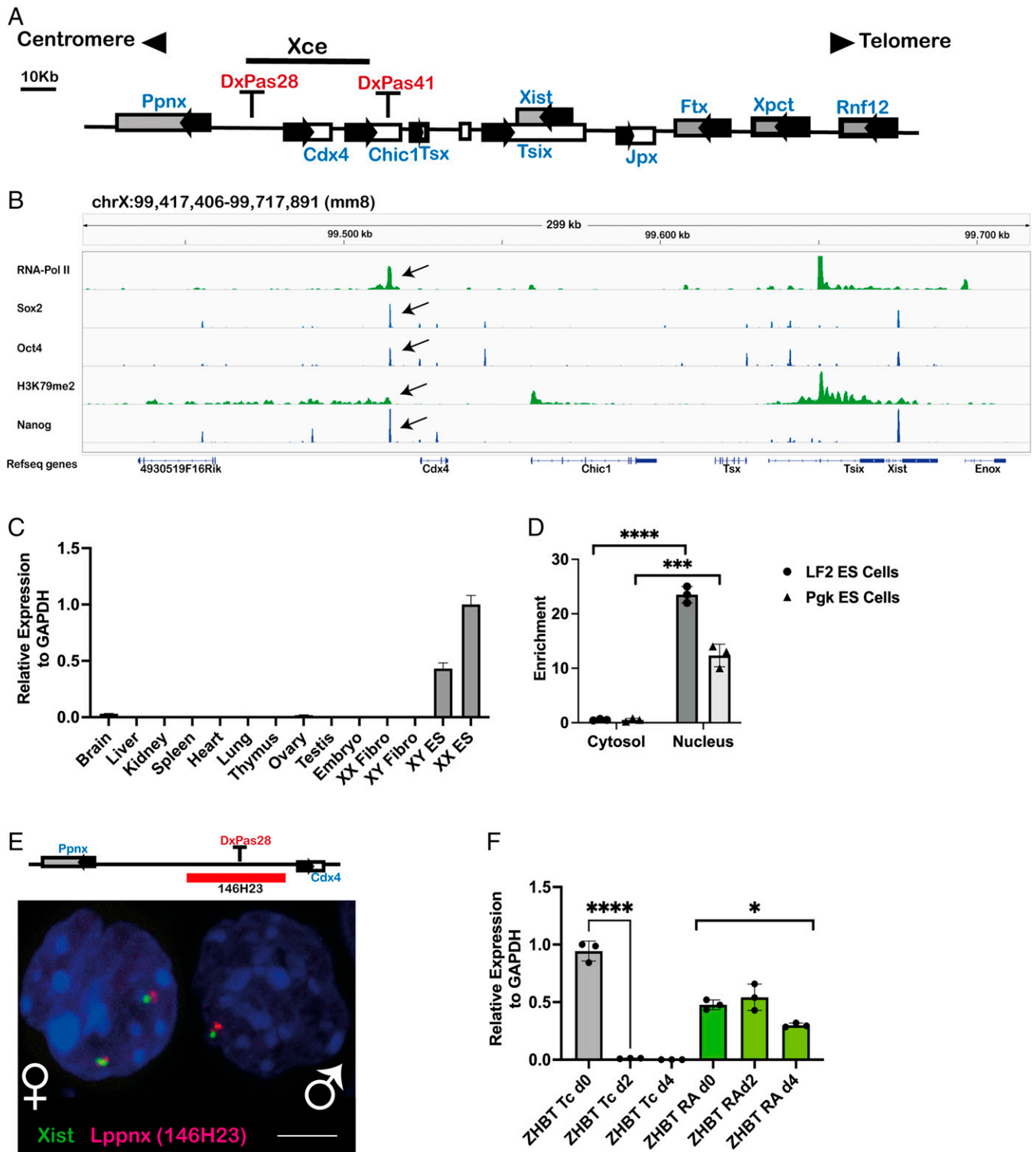


Fig. 1. A long noncoding RNA is transcribed from the predicted X-controlling element. Schematic view of the X-inactivation center with the predicted Xce indicated by a black bar (A). ChIPseq analysis shows a clear signal, marked with a black arrow, for the pluripotency factors Oct4, Nanog and Sox2 within the Xce. RNA-Pol II and H3K79m2 indicate initiation and maintenance of active transcription (B). The transcript identified in B is mainly expressed in mouse male and female ES cells but not in differentiated cells, as exemplified by organ analysis of adult mice. Relative expression levels of the transcript were measured by qRT-PCR in mouse organs, embryos, and cell lines. XX Fibro: Female fibroblast cell line, XY Fibro: Male fibroblast cell line. XX ES: Female embryonic stem cell line XY ES: Male embryonic stem cell line. (C). Fractionation of cytosol and nuclei in two ES cell lines, LF2 and Pgk, reveals the localization of the transcript to be mainly in the nucleus, indicating a bona fide lncRNA transcript. Enrichment in the two compartments was measured using qRT-PCR. Two-sample *t* test: $P < 0.0001$ (LF2), $P = 0.0006$ (Pgk) (D). Visualization of the transcript in the nucleus of male and female ES cells using RNA-FISH. The position of the BAC used as FISH probe is highlighted as a red bar (E). The expression of the transcript depends on Oct4. Oct4-deficient ES cell line (ZHBT) which carries a tetracycline-repressible Oct4 transgene was differentiated either in the presence (RA) or absence (TC) of Oct4. In the absence of Oct4 (Tc) the transcript is rapidly down-regulated during differentiation, whereas the maintenance of Oct4 during differentiation (RA) maintains also the transcription. Transcript levels are shown relative to glyceraldehyde-3-phosphate dehydrogenase (GAPDH). Two-sample *t* test: $P < 0.0001$. One-way ANOVA: $P = 0.0143$ (F).

presence of Oct4 its expression was maintained during differentiation (Fig. 1*F*). These results indicate that the transcript is down-regulated during the differentiation of ES cells and that Oct4 is required for its expression.

In summary, we show evidence that inside the predicted *Xce* region is localized the origin of a novel putative long noncoding RNA, which is expressed in male and female ES cells as well as in the ICM of late blastocysts. Since during differentiation the transcript is down-regulated, its expression pattern is compatible with the notion that pluripotency factors are required/involved in its expression. Given that the predicted genomic region of the transcript intermingles with the previously defined and published *Ppnx* gene, we named the transcript long noncoding RNA in the *Ppnx* gene, *Lppnx*.

Lppnx Is Differentially Expressed in Hybrid ES Cells during Differentiation. The choice of which chromosome will be inactivated is made very early upon differentiation. Since we had shown *Lppnx* is down-regulated during differentiation (Fig. 1*F*), we took a closer look of the exact timepoint and allele specificity of *Lppnx* expression during differentiation of ES cells using single cell RT-qPCR on hybrid 129Sv/Pgk1a female ES cells. The use of allele-specific primers allowed the expression of *Lppnx* on the respective (129 or Pgk1a) X chromosome to be followed. In the pluripotent state these cells express distinct allele-specific levels of *Lppnx*: in a majority of cells, *Lppnx* from the 129Sv X chromosome is more highly expressed than from the Pgk1a allele (*SI Appendix*, Fig. S2, d0). This ratio reverses by day 1 of differentiation; that is, by the time that choice of the X to be inactivated is established, with higher numbers of cells expressing from the strong (Pgk1a) *Lppnx* allele (*SI Appendix*, Fig. S2, d1). By day 2 most of the cells had silenced *Lppnx*. Interestingly, at day 1 the percentage of cells showing predominant expression from the Pgk1a (strong) allele at 61% compared to 32% from the 129Sv (weak) allele approximates inversely the X-linked gene expression ratio found later in heterozygous *Xce* crosses (75 vs. 25%). This may indicate that *Lppnx* expression is linked to *Xist* expression and involved in the choice of which X is to be inactivated.

Deletion of the Putative Promoter Sequence of *Lppnx* Abolishes the Expression of *Lppnx* RNA in ES Cells and Embryos. To support the idea of a putative promoter region both required and sufficient for the expression of *Lppnx*, we deleted this element in 129Sv mice using CRISPR/Cas9 (Fig. 2*A* and *SI Appendix*, Fig. S1 *C* and *D*). Phenotypically, female and male mice carrying either homo- or hemizygous deletions do not show obvious abnormalities. In addition, female ES cells generated from crosses of these mice are morphologically normal and exhibit normal levels of the ES cell pluripotency marker Oct4 (Fig. 2*B* and *C*). However, upon differentiation, *Xist* levels were found to be two- to three-fold higher compared to WT ES cells (Fig. 2*D* and *E*). Male ES cells carrying the deletion similarly exhibited increased *Xist* levels and, as a consequence, increased *Xist* foci after differentiation (Fig. 2*F* and *G*). Interestingly, the levels of the pluripotency marker *Rex1* are moderately higher in undifferentiated hetero and homozygous female ES cells, whereas differentiation capacity indicated by the induction of the neuronal marker *Nestin* is not affected by the deletion of *Lppnx* (Fig. 2*D*). In summary, the deletion of the predicted promoter region leads to a complete silencing of *Lppnx* transcription and to increased levels of *Xist* after differentiation of such male and female ES cells.

The Phenotypic Effect of the Deletion of the Entire 80-kb *Xce* Candidate and the 600-bp *Lppnx* Promoter Are Very Similar.

We have shown that the deletion of *Lppnx* leads to increased *Xist* levels in 129Sv male and female ES cells during differentiation. Given the robust phenotype shown in male ES cells (*Xist* RNA level and *Xist* foci), we decided to compare this phenotype with a deletion of the entire *Xce* candidate region and finally with the entire *Xce* except the *Lppnx* region. Using CRISPR/Cas9 we introduced the deletions in WT 129Sv ES cells (Fig. 3*A*). Upon differentiation we observed that the 80-kb and the 600-bp lines show a comparable phenotype in terms of *Xist* levels and foci. In contrast, the deletion of the protein coding genes *Cdx4* and *Chic1* does not have any effect on *Xist* levels after differentiation (Fig. 3*B–D*). From this result, we conclude that *Lppnx* is the driving factor in the formation of the observed phenotype.

Heterozygous Deletion of *Lppnx* in a *Xce* Heterozygous Background Influences the Choice of the X Chromosome To Be Inactivated.

The *Xce* locus is associated with the introduction of bias in choice of which X will be inactivated. To test the influence of *Lppnx* on this, we crossed mice heterozygous for *Xce* carrying a deletion of or not, of *Lppnx*. As a readout we isolated E10.5 female embryos and performed X chromosome allele-specific RT-qPCR to calculate a quantitative ratio for XCI (Fig. 4*A*). F1 embryos derived from crossings of 129Sv (*Xce^f*) and HPRT-Pgk1a (*Xce^f*) showed a calculated expression ratio for *Xist* of 1.64 (Fig. 4*B*). Conversely, expression ratios of two representative X-linked genes were 0.64 and 0.78, respectively. The deletion of *Lppnx* in 129Sv embryos shifted the *Xist* allelic ratio to 2.42, whereas the ratios of X-linked genes decreased to 0.54 and 0.49, respectively (Fig. 4*B*). These data suggest that the deletion of *Lppnx* on an *Xce^f* haplotype background influences the choice process in XCI in *Xce* heterozygous embryos. Moreover, it suggests that *Lppnx* expression may prevent X inactivation by repressing *Xist* up-regulation (Fig. 4*B*).

The Deletion of *Lppnx* in a *Xce^f* Strain Shows Only Weak Effects.

Given the effect described above we expected to observe a similar phenotype when deleting *Lppnx* on a *Xce^f* carrying mouse strain. However, analysis of *Hprt-Pgk⁻/129Sv⁺* embryos carrying such deletions failed to show any significant effect on *Xist* ratios compared to WT (Fig. 4*B*). This would suggest that *Lppnx* is either not active or only weakly active in *Xce^f*-carrying strains. Intriguingly, the ratio in double-knockout (ko) embryos showed almost identical values to that of WT littermates. If the deletion of *Lppnx* had no effect on the *Xce^f* strain, then the observed ratio would be expected to be similar to that of heterozygous embryos carrying a deletion on the 129Sv X, rather than having values similar to those of WT. These data were confirmed by the observations of male *Xce^f* ES cells after differentiation. The deletion of *Lppnx* leads to an up-regulation of *Xist* and to an increase of *Xist* foci; however, both to a much weaker degree compared to male *Xce^f* ES cells (*SI Appendix*, Fig. S3).

The *Lppnx* Promoter Region Interacts with *Xist* Intron1. Higher order chromatin interactions are known to play a crucial role in XCI (38). We analyzed published Hi-C data for possible interactions of the *Lppnx* locus with elements of the *XIC* which might help to explain the observed phenotypes using an epigenome browser (epigenomegateway.wustl.edu/browser/). The visualization of interactions within the *XIC* and the predicted *Xce* locus revealed a possible connection between the loci of *Lppnx*

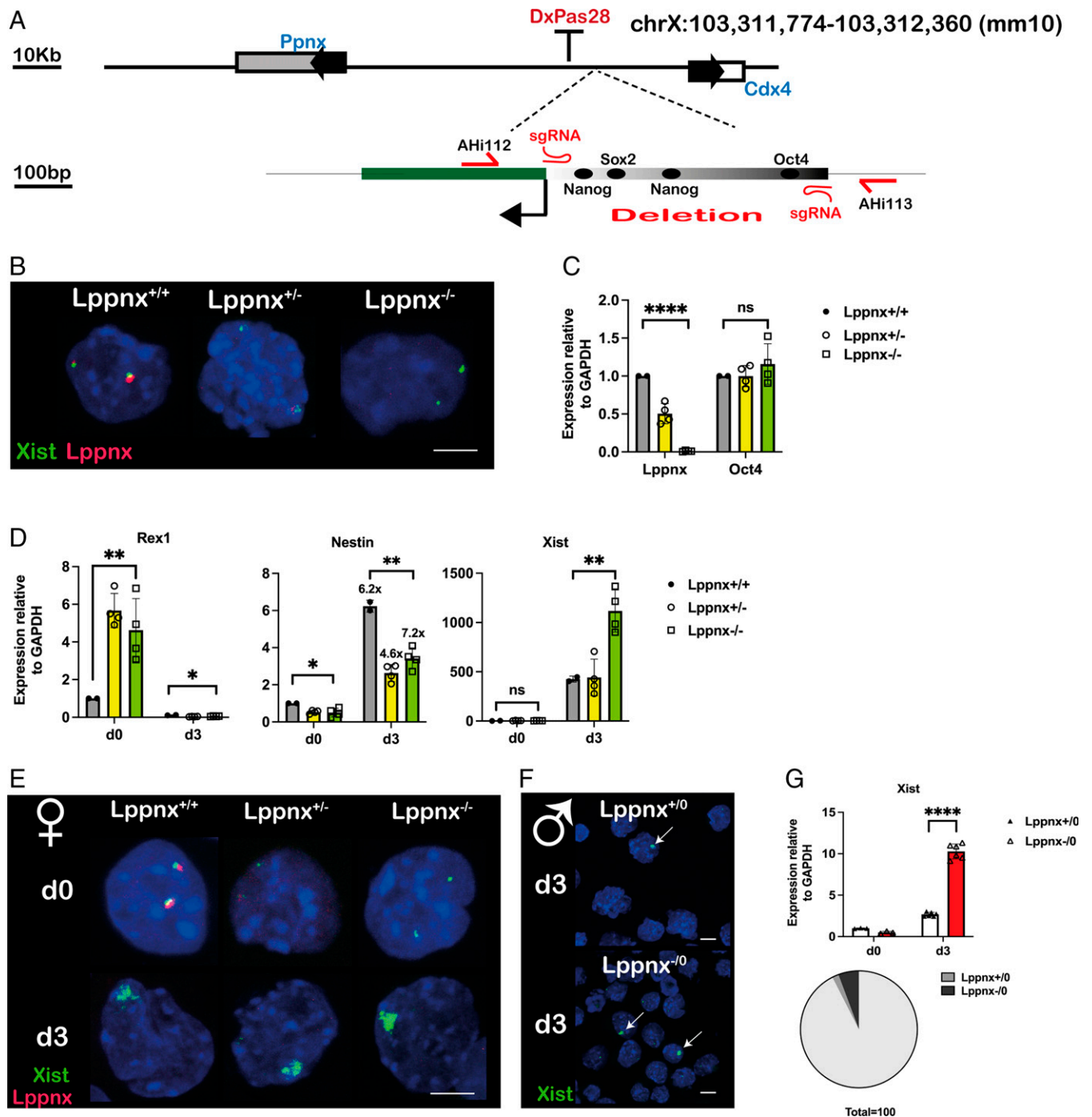


Fig. 2. Deletion of the putative promoter sequence of *Lppnx* in 129Sv mice. CRISPR/Cas9 mediated genome editing was used to delete the 595-bp promoter fragment in mice. Schematic view of the position of the sgRNAs and the primer used for subsequent genotyping of the founder animals (A). FISH analysis of female ES cells generated from *Lppnx* Δ 600 mice show the absence of a signal for *Lppnx* indicating that the predicted promoter fragment drives *Lppnx* expression (B). *Lppnx* expression is down-regulated in heterozygous ES cells and absent in homozygous cells carrying the deletion of the putative promoter region. Two-sample *t* test: $P < 0.0001$ (comparing WT with homozygous cells). The absence of *Lppnx* expression does not affect pluripotency in these ES cells as shown by a comparison of Oct4 expression levels. One-way ANOVA: $P = 0.4998$ (C). Female ES cells homo- and heterozygous for the deletion of *Lppnx* show different levels of key markers compared to WT cells upon differentiation. Cells were analyzed at day 3 after onset of differentiation (see *Materials and Methods* section). *Rex1* levels are elevated in both, homozygous and heterozygous undifferentiated cells. Two-sample *t* test: $P = 0.0023$. After differentiation *Rex1* is down-regulated in all three lines. One-way ANOVA: $P = 0.008$. *Nestin* was used as a differentiation marker. The degree of differentiation was calculated as fold change in expression of *Nestin*. The fold change is given above the bars in d3. All three lines show comparable fold changes during differentiation. Two-sample *t* test: $P = 0.0242$ (d0) $P = 0.0032$ (d3). *Xist* expression is markedly increased after differentiation in homozygous cells. d0: One-way ANOVA: $P = 0.4959$. d3: Two-sample *t* test between WT and homozygous deletion $P = 0.0064$ (D). RNA-FISH analysis of differentiated female ES cells shows an increased intensity of *Xist* associated clouds upon *Lppnx* depletion, in agreement with the analysis in D (E). Accordingly, male ES cells deficient for *Lppnx* express higher *Xist* levels after differentiation as shown by qRT-PCR and the elevated number of *Xist* clouds indicated by arrows (F, G). Two-sample *t* test: $P < 0.0001$. The increase of *Xist* clouds in ES cells deficient for *Lppnx* compared to WT cells is visualized in a pie chart (G).

and *Xist* Intron1 (XI1) in both male and female ESCs (Fig. 5A). It has been shown that this Intron contains binding sites for pluripotency factors, playing a crucial role in XCI (18). Interestingly,

Intron 1 seems to be dispensable for XCI *in vivo* and *in vitro* but it may be involved in the choice of which X is inactivated in female cells (39).

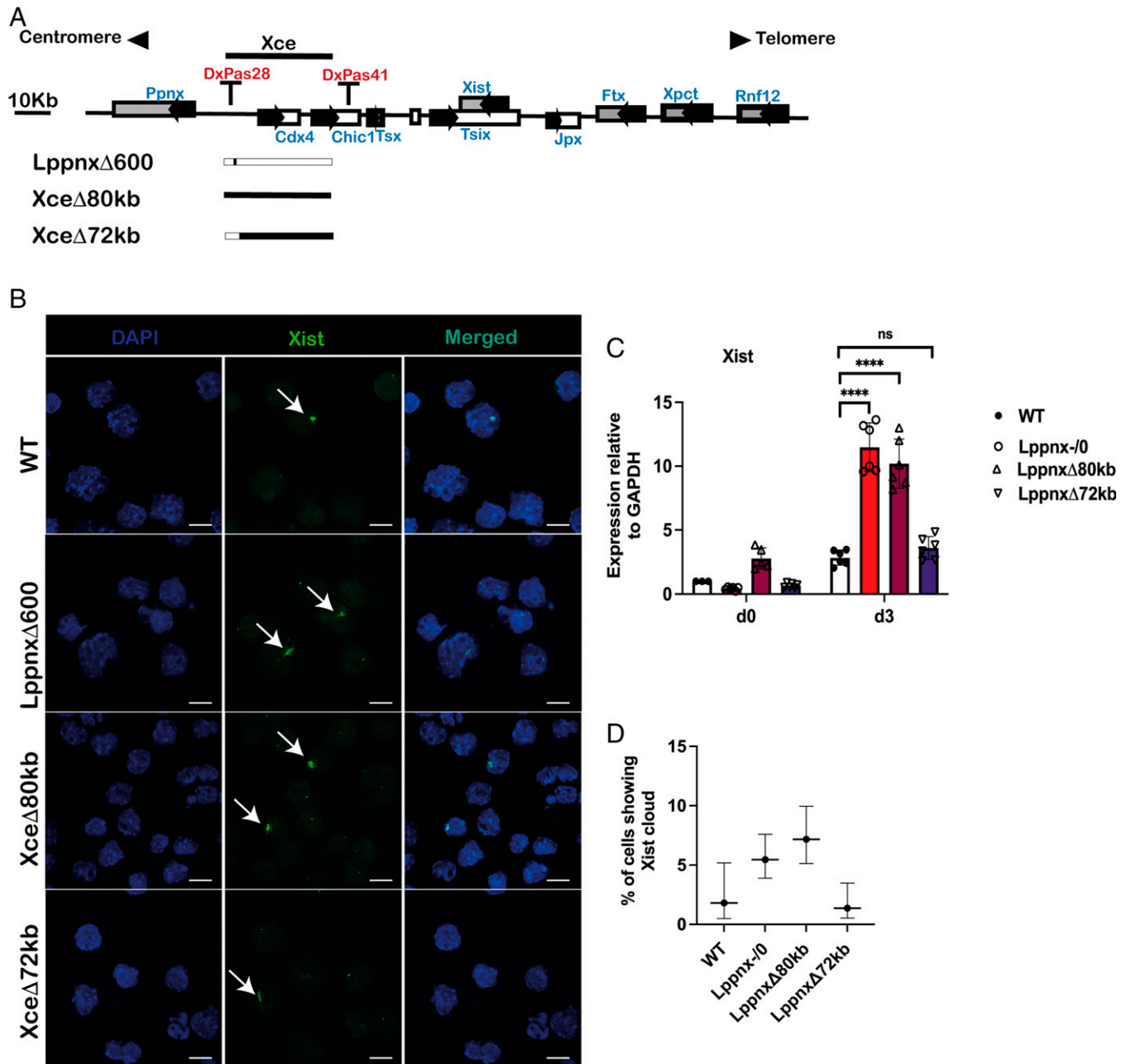


Fig. 3. Comparison of the number of Xist clouds in male ES cells. Schematic view of the X inactivation center and the CRISPR mediated deletion. 129Sv male ES cells were used to introduce a deletion of the entire predicted *Xce* (*Xce*Δ80kb) or a deletion which leaves intact the *Lppnx* region (*Lppnx*Δ72kb). These cell lines were compared with a WT and the previously shown *Lppnx*Δ600 (corresponding to *Lppnx*-0) cell line (A). After differentiation *Xce*Δ80kb and *Lppnx*Δ600 show elevated numbers of Xist clouds whereas *Lppnx*Δ72kb and WT show comparable levels (B). qRT-PCR analysis of the cells in B showed elevated Xist expression levels in *Xce*Δ80kb and *Lppnx*Δ600 but not in *Lppnx*Δ72kb compared to WT. Two-sample *t* test: $P < 0.0001$ (C). Quantification of Xist clouds shown in B are given in percentage of Xist clouds within the different cell lines. Remarkably, only *Xce*Δ80kb and *Lppnx*Δ600 show elevated ratio of clouds, whereas *Lppnx*Δ72kb and WT cells show comparable levels. Percentages are given with an upper and lower level and are shown with a CI of 95% (Wilson/Brown) (D).

Deletion of the Pluripotency Factor Binding Region of Xist Intron1 Rescues the Phenotype in Lppnx KO Male ES Cells. We decided to use CRISPR mediated ablation of the pluripotency factor binding region of Xist Intron1 in *Lppnx* deficient 129Sv male ES cells, based on data obtained from (18), to test whether this has any effect on the elevation of Xist levels observed in these cells (Fig. 5B). Elevated Xist levels are observed in *Lppnx* ko cells as reported earlier; however, analysis of three independent clones carrying a *Lppnx*/Xist Intron1 double ko showed a complete rescue of the phenotype leading to Xist levels after differentiation comparable to those of wildtype (WT) cells (Fig. 5C).

Lppnx Controls the Loading of Pluripotency Factors at Xist Intron1 and DxPas34. As mentioned, transcription factors bound to XI1 modulate Xist expression and probably choice during XCI. We analyzed the loading of three key factors on XI1. Oct4 and Rex1 have been shown to repress Xist expression (18), whereas YY1 acts as a transcriptional activator of Xist (40). We used ChIP-seq to analyze the loading of these factors in WT and *Lppnx* ko ES cells. We found that upon *Lppnx* depletion, the loading of Oct4 and Rex1 at XI1 decreased markedly in *Xce*^{fl} as well as in *Xce*^{fl} ES cells, whereas YY1 binding remained unchanged (Fig. 5D and SI Appendix, Fig. S4A). These data may indicate that *Lppnx* controls the level of bound transcription

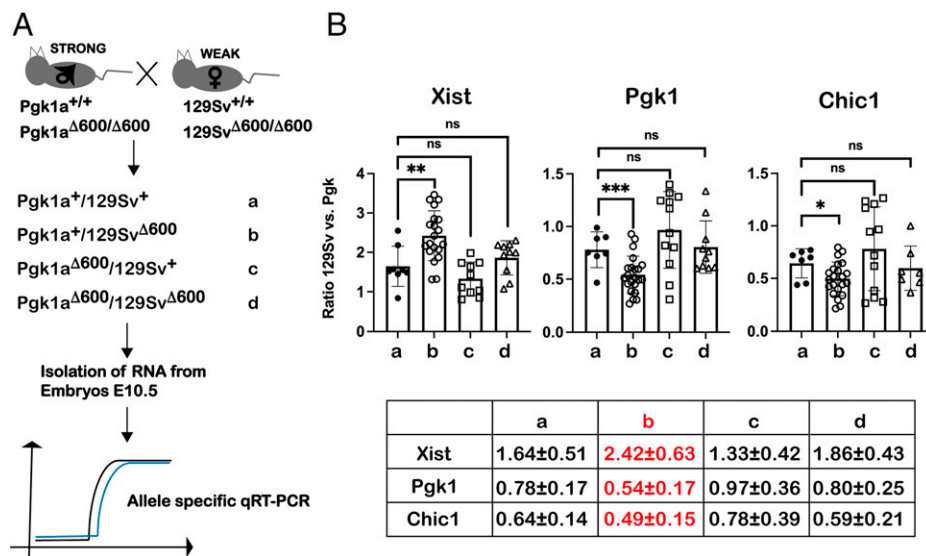


Fig. 4. Deletion of *Lppnx* promotes a shift in X-linked expression ratio in heterozygous embryos. Schematic view of the breeding strategy used to analyze X-linked expression ratios. From heterozygous *Xce* crosses between *Xce^w* (weak, 129Sv) and *Xce^s* (strong, *Pgk1a*), indicated from *a–d*, E10.5 female embryos were isolated. $\Delta 600$ corresponds to the 600-bp promoter deletion shown before. We used allele-specific qRT-PCR to define the X-linked expression ratio as follows: $2^{Ct(Pgk)-Ct(129)}$ (A). Reciprocal crosses of *Xce^s* with *Xce^w* with or without a depletion of *Lppnx* show a significant shift of *Xist* ratio as well as of X-linked genes. *Pgk1* and *Chic1* in E10.5 embryos only in *Xce^s-Lppnx Δ 600/*Xce^w* embryos, whereas all other combinations are comparable to WT. Two-sample *t* test *Xist*: $P = 0.0048$, *Pgk1*: $P = 0.0042$, *Chic1*: $P = 0.0379$. Each dot in the plots represents the value of a single embryo measured in three technical replicates. Expression ratios are summarized in a table, only crossing *b* (marked in red) shows significant difference to WT (B).*

factors which determine the onset of *Xist* up-regulation and hence the choice of which X will be inactivated. Interestingly, the transcription factor *Rex1* evolved by retro-position from the *YY1* gene. *Rex1* binds targets divergent from *YY1*, but the binding motifs of *Rex1* and *YY1* show similarity in their core region (41). Considering this, *YY1* and *Rex1* may compete for binding on *XI1*, although *YY1* binding seemed unchanged.

Similar observations can be carried out at the microsatellite repeat *DxPas34*, an important control region for the expression of *Tsix* (42). While on both *Xce* backgrounds binding of *Oct4* decreased slightly upon the deletion of *Lppnx*, *Rex1* showed a very different and divergent pattern: while in *Xce^s* cells there was a decrease in loading, cells from *Xce^w* showed increased loading for *Rex1* upon *Lppnx* depletion (Fig. 5D). This result may explain differences in the phenotype of the *Lppnx* ko in *Xce^s* and *Xce^w* ES cells. Increased binding of *Rex1* at *DxPas34* in *Xce^w* ES cells would maintain *Tsix* transcription and hence compensate for the loss of *Oct4* in *XI1*. In contrast, the low level of *Rex1* at *DxPas34* in *Xce^s* cells leads to decreased *Tsix* transcription and together with decreased *Oct4* level at *XI1*, to an enhanced activation of *Xist* transcription.

Discussion

The most widely discussed and shared idea about how the *Xce* influences choice in XCI is that this genetic region serves to bind a series of autosomal factors which in turn would regulate the main defined players in XCI, *Tsix* and *Xist* (43, 44). In the present study, we define the *Xce* as an 80-kb spanning region between the microsatellite repeats *DxPas28* and *DxPas41*. We identified *Lppnx*, a lncRNA originating from within this region, as a novel candidate for the *Xce* locus and suggest a mechanism involving modulation of the occupancy of pluripotency factors at *Xist* Intron1 and *DxPas34*, two key regions in XCI. Our analysis suggests that different binding capacities of pluripotency factors at *Xist* Intron1 and *DxPas34* influence *Xist* up-regulation and most likely the choice in XCI, a hypothesis which has been presented recently (39). Our results extend this idea by showing that

Lppnx can modulate the binding of these factors in a background-dependent manner. In particular, *Oct4* and *Rex1* showed decreased binding at Intron1 upon deletion of *Lppnx*. Since *Oct4* was shown to inhibit *Xist* up-regulation, this reduced binding could well explain the increased expression of *Xist* after differentiation on an *Xce^s* background (18). This effect is counteracted in *Xce^w* ES cells by increased binding of *Rex1* at *DxPas34*, which in turn maintains *Tsix* transcription and inhibits the *Xist* up-regulation (19).

Whereas the *Xce^s* allele studied here (129Sv strain) is highly susceptible to the lack of *Lppnx*, the *Xce^w* strain (HPRT-*Pgk1a*) shows a weaker phenotype upon the ablation of *Lppnx*. In both strains, *Lppnx* modulates *Xist* expression most likely by controlling the occupancy of *Oct4* and *Rex1* (and possibly other factors) in *Xist* Intron1. *Lppnx* expression itself is highly dependent on the presence of *Oct4*, linking *Lppnx* expression to pluripotency and XCI and forming a feedback loop between *Lppnx* and *Xist* (*SI Appendix*, Fig. S4B). This association may explain why in previous studies it has been supposed that the *Xce* might be identical to *Xist* (33). Our analysis shows clearly not only that *Xce* is genetically different from *Xist*, but also provides a likely mechanism for how *Xce* acts as a *Xist* repressor with the requirement of *Xist* Intron1.

The question of how *Lppnx* modulates the binding of transcription factors at a molecular level remains to be elucidated. Emerging results from previous studies stress the possible role of lncRNAs as molecular scaffolds (45, 46). For *Lppnx* to act as a scaffold, binding pluripotency factors for *XI1* would require an interaction or proximity between the *Lppnx* and *Xist* locus. Analysis of published Hi-C and 5C data suggests that indeed both loci do interact, underlining the importance of topologically associating domains in long-range chromatin interaction in many biological phenotypes (38, 47). The zinc-finger protein CTCF and the cohesion complex are the main players in the establishment of both, long- and short-range chromatin interaction (48). While both the *Lppnx* promoter and *Xist* Intron1 contain binding sites for both factors, the extensive genetic heterogeneity between *Xce^s* and *Xce^w* strains might lead to modulation of binding and hence different chromosomal conformations. The same is true

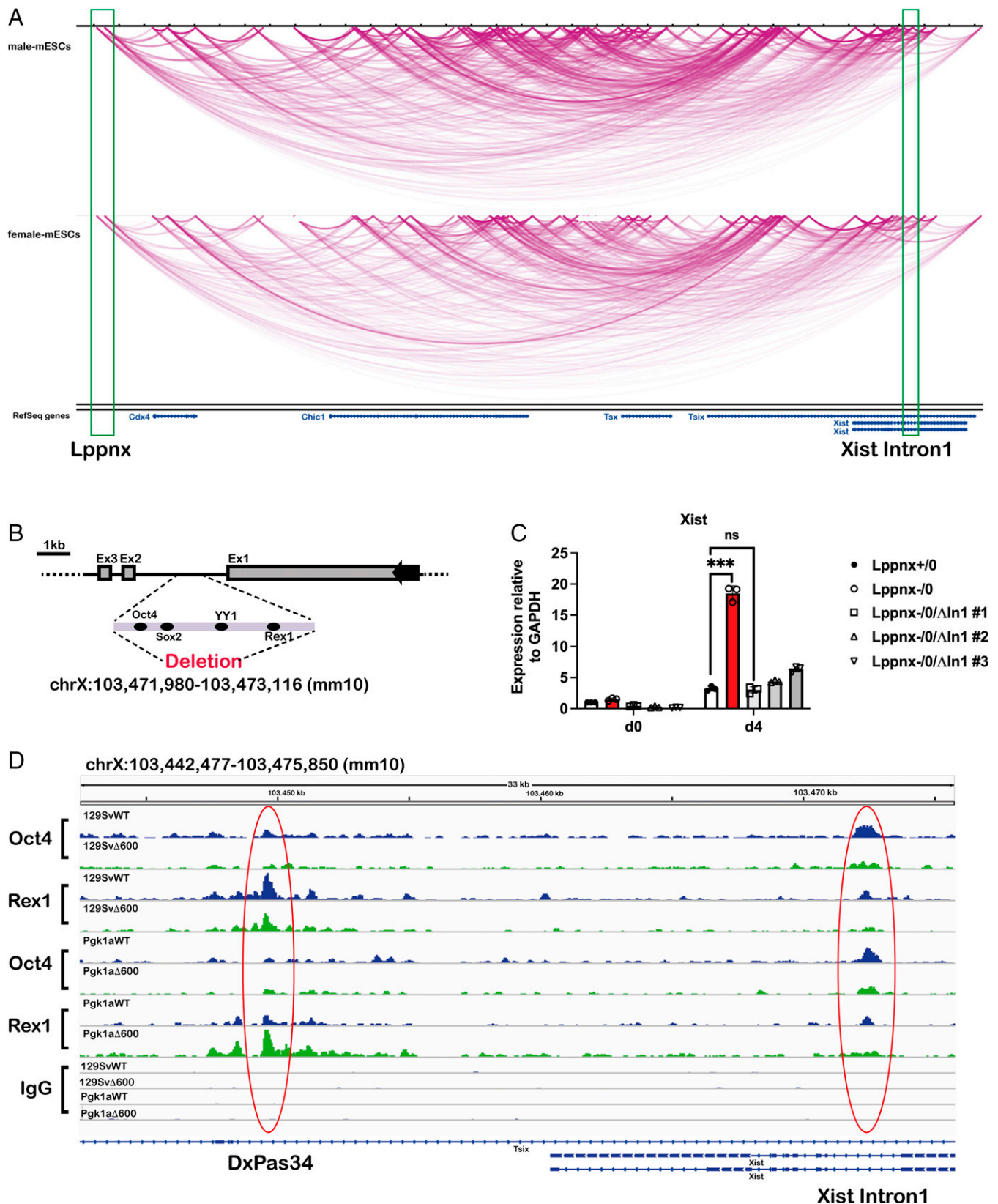


Fig. 5. The *Lppnx* locus may interact with *Xist* Intron1 in mouse ES cells and controls the loading of Oct4 and Rex1 in Xi1. Screenshot of a Hi-C analysis showing a part of the X inactivation center including *Xist* and *Lppnx*. The green rectangles indicate the transcription start site of *Lppnx* and *Xist* Intron1 showing a possible interaction between these two regions in both, male and female ES cells (A). Schematic view of the pluripotency factor binding region of *Xist* intron 1 which was deleted in 129Sv and 129Sv Δ^{600} male ES cells, respectively, using CRISPR (B). Elevated *Xist* expression observed in 129Sv Δ^{600} male ES cells (*Lppnx*-/*0*) after differentiation is completely reversed after the deletion of *Xist* Intron1. Three independent lines (#1, #2, #3) are shown. Two-sample *t* test $P = 0.001$ (C). *Lppnx* regulates the loading of pluripotency factors in *Xist* Intron1 and *DxPas34*. ChIPseq experiments show that upon deletion of *Lppnx* the loading of Oct4 and Rex1 is reduced at *Xist* Intron1 (red circle, Right) in male 129Sv and Pgc1a ES cells. In contrast, Rex1 binding at *DxPas34*, a regulatory region of *Tsix*, is reduced in *Lppnx*-deficient 129Sv ES cells, whereas in Pgc1a cells Rex1 binding is increased (red circle, Left) (D).

for pluripotency binding sites in *Xist* Intron1 and the *Lppnx* promoter regulating the level of *Lppnx* expression (*SI Appendix, Fig. S4B*).

Recently it was reported that the promoter region of the non-coding RNA *Linx* (*LinxP*) acts as a cis-regulatory element and long-range silencer to influence the choice of X chromosome to be inactivated independent of its transcriptional activity (49). We believe that *Lppnx* and *Linx* are mostly identical concerning their positions on the X chromosome. However, we think that both transcription and the lncRNA itself play an important role in the interpretation of the results shown here. For one to fully understand the function of a lncRNA, it is important to identify its interacting partners, and in recent years lncRNA-protein interactions have gained increased attention. We analyzed CLIP-Seq data from mouse embryonic stem cells and found that Oct4 binds to *Lppnx* in these cells, whereas YY1 shows a neglectable signal (*SI Appendix, Fig. S5*, blue boxed region) (50). Interestingly, both Oct4 and YY1 seem to bind to *Tsix* but not to *Xist* (*SI Appendix, Fig. S5*, red boxed region). These data may indicate that upon a certain proximity between the *Lppnx* and the *Xist/Tsix* locus, the *Lppnx* RNA provides a pool of Oct4 (and other factors) to the regulatory regions in the *Xist/Tsix* locus. Hence, lack of *Lppnx* RNA leads to decreased Oct4 occupancy in important regulatory regions like *Xist* Intron1 and *DxPas34*. These results indicate that the binding of important transcription factors in XCI can be directly regulated by *Lppnx*. The quantitative binding of Oct4 (and other factors) to *Lppnx* strongly depends on the sequence of the RNA. Therefore, we analyzed possible splice variants of *Lppnx* in *Xce^a* and *Xce^c* ES cells, which may explain the differential loading of these factors to the prospective binding sites. Indeed, we found splice variants predominantly occurring in *Xce^a* but not in *Xce^c* and vice versa (*SI Appendix, Fig. S6*). This finding brings another level of complexity into the action of *Lppnx*, suggesting that different splice variants result in differential loading of the transcription factors.

Our results and the model that results suggest that the action of *Xce* is quite complex, in agreement with the rather quantitative and variable effects of *Xce* action on X-inactivation ratios observed in in vivo experimental typing systems. Indeed, characterization of unknown *Xce* alleles historically has been based on extended testing of progeny from crosses involving various known *Xce* tester strains, precisely to deal with this variability. The characterization of *Lppnx* as shown here could facilitate substantially the categorization of *Xce* strains. However, additional efforts will be needed to determine its role within the complex network acting through the *Xce*. This suggests the question of whether *Lppnx* acts in concert with additional factors so far not identified. Future research will center on questions concerning the possible binding of Oct4/Rex1 to *Lppnx*, the role of different isoforms of *Lppnx* and their implications for differential factor binding, and a more extensive exploration of individual *Xce* allele variability and its mechanistic implications.

Materials and Methods

Generation of *Lppnx* KO Mice. To generate a transgenic mouse line with the promoter of *Lppnx* deleted we used CRISPR (clustered regularly interspaced short palindromic repeats)-Cas9 to target this region in the mouse zygote. For a more detailed description please refer to *SI Appendix, SI Methods*.

CRISPR-Mediated Genome Editing in ES Cells. Using <https://horizondiscovery.com/en/ordering-and-calculation-tools/crispr-design-tool>, we identified suitable target sequences with minimal off target effects for sgRNA synthesis. Corresponding oligonucleotides (listed in *SI Appendix, Table S1*) were then cloned into pSpCas9(BB)-2A-GFP (PX458, a gift from Feng Zhang, addgene #48138)

(51) using the BbsI site. The plasmids were then transfected in ES cells (Xfect, Takara #631317) followed by fluorescence activated cell sorting of green fluorescent protein-positive cells. Single clones were analyzed by PCR with primer pairs listed in *SI Appendix, Table S1*.

Generation of ES Cell Lines from Blastocysts and ES Cell Differentiation. Flushed E3.5 blastocysts were cultured for 12–24 h in KSOM media (Invitrogen). Before hatching they were then transferred in gelatinized 96-well dishes containing normal cell culture media supplemented with 2i, Lif, and 10% serum (52). After several days round colonies were obtained and expanded by continuous dissociation.

ES cell differentiation was carried out as previously described (53). Briefly, 1 million cells were plated on a 6-cm dish coated with laminin. After 6 h Fgf2 was added to the cells. The medium was replaced every day and cells were harvested after 3 d of differentiation.

Nuclei Extraction of ES Cells. Cells were grown until confluency, trypsinized, and washed with phosphate-buffered saline. The cell pellet was resuspended in a hypotonic buffer (10 mM Hepes, 1.5 mM MgCl₂, 10 mM KCl, 0.5 mM DTT, 0.05% Nonidet P-40, +protease inhibitors) and incubated 20 min on ice. After centrifugation, supernatant and the nuclei were subjected to RNA isolation.

RNA Isolation and cDNA Synthesis. RNA from tissue, embryos, and cells was isolated using the Qiagen RNeasy kit according to manufacturer instructions. cDNA synthesis was carried out using 1 µg of total RNA and the SuperScript III First-Strand Synthesis System (Invitrogen#18080-051). Residual genomic DNA was removed by applying a suitable DNase (Thermo #EN0771).

RNA FISH on ES Cells and Preimplantation Embryos. RNA FISH on ES cells was carried out according to published protocols (54) with the following modification. ES cells were fixed in ice-cold paraformaldehyde for 5 min before being spotted on glass slides. RNA FISH on blastocysts was performed following published protocols (55).

Z-stacks were captured on a Leica SP5 confocal microscope (Leica Microsystems, Germany) and images were prepared with Fiji/ImageJ software.

Single-Cell Gene Expression Analysis. Single-cell gene expression analysis was performed as described previously (56) and as recommended by Fluidigm <https://www.fluidigm.com/area-of-interest/single-cell-analysis/single-cell-analysis-with-microfluidics#> (www.fluidigm.com/single-cell-expression.html; South San Francisco, CA, USA). For a more detailed description please refer to *SI Appendix, SI Methods*.

qRT-PCR Using Allele-Specific Primer and Calculation of Expression Ratios. The solution from cDNA synthesis was diluted 1:40 and from this 5 µL was mixed with 2× QPCR BIO SYGREEN MIX LO-ROX reagent (PCR BIO) for every single reaction. The sequences of primer are shown in *SI Appendix, Table S1*. Expression ratios have been defined as following: $2^{\text{Ct(Pgk)-Ct(129)}}$. Statistical analysis was performed using JMP and Prism software.

Chromatin Immunoprecipitation and Sequencing (ChIP-Seq). This protocol was adapted from a CUT&RUN Protocol from EpiCypher (<https://www.epicypher.com/content/documents/protocols/cutana-cut&run-protocol.pdf>) and is based on the use of magnetic beads. For a more detailed description please refer to *SI Appendix, SI Methods*.

ChIP-Seq Data Processing. Data were processed on Galaxy. Adapters were removed with Trimmomatic v0.36.6 and sequences having an average quality below 20 were eliminated. Quality statistics were verified with Fastqc v0.69. Reads were aligned to mm10 using Bowtie2 v2.3.4.2 using default parameters. Bam files were ordered by coordinates with SortSam v2.7.1.1. Only reads mapping to the main chromosomes were kept. Unmapped and nonprimary reads were removed with Samtools v1.1.2 ("Filter SAM or BAM, output SAM or BAM"). Duplicated reads were removed with picards tools v2.7.1.0 (MarkDuplicatesWith-MateCigar). Bigwig files were generated with bamCoverage v2.5.7.0 normalizing to 1× coverage on mm10 and extending reads to 150 bp.

Hi-C Data. Using an epigenome browser (epigenomegateway.wustl.edu/browser/) we analyzed published Hi-C data obtained from male and female ESC (38). The GEO accession number for the datasets are GSM873934 (male-mESCs) and GSM873927 (female-mESCs).

CLIP-Seq Data. Data sets were downloaded using the Geo database (<https://www.ncbi.nlm.nih.gov/geo/>) with the respective accession numbers: Oct4 (GSE68196) and YY1 (GSM1665564). Integrative Genomics Viewer (IGV, Broad Institute) was used to visualize the data.

Data Availability. All study data are included in the article and/or *SI Appendix*.

ACKNOWLEDGMENTS. We thank Jamie Hackett and Matthieu Boulard from EMBL Rome for critical reading of the manuscript and valuable comments; Neil Humphreys and Neil Dear from the Transgenic Facility of EMBL Rome for generating multiple knock-out mouse lines; Giulia Bolasco and Monica Di Giacomo for

guiding us through analytical microscopy; and Philip Hublitz and James Sawitzke for advice in cloning transgenic vectors. The bio-informatic analysis was carried out by Nicolas Descostes.

Author affiliations: ^aEpigenetics and Neurobiology Unit, EMBL Rome, Monterotondo, 00015, Italy; ^bGenomics and Epigenomics of Animal Development, Developmental and Stem Cell Biology Department, Institut Pasteur, 75015 Paris, France; ^cBlizard Institute, Barts and The London School of Medicine and Dentistry, Queen Mary University of London, London, E1 2AT, United Kingdom; and ^dMammalian Genetics Unit, MRC Harwell, Oxfordshire OX11 0RD, United Kingdom

1. J. E. Mank, The W, X, Y and Z of sex-chromosome dosage compensation. *Trends Genet.* **25**, 226–233 (2009).
2. S. Ercan, Mechanisms of x chromosome dosage compensation. *J Genomics* **3**, 1–19 (2015).
3. M. I. Kuroda, A. Hilfiker, J. C. Lucchesi, Dosage compensation in *Drosophila*-a model for the coordinate regulation of transcription. *Genetics* **204**, 435–450 (2016).
4. B. Payer, J. T. Lee, X chromosome dosage compensation: How mammals keep the balance. *Annu. Rev. Genet.* **42**, 733–772 (2008).
5. M. Leeb, A. Wutz, Mechanistic concepts in X inactivation underlying dosage compensation in mammals. *Heredity* **105**, 64–70 (2010).
6. E. Heard, C. M. Distech, Dosage compensation in mammals: Fine-tuning the expression of the X chromosome. *Genes Dev.* **20**, 1848–1867 (2006).
7. N. Brockdorff, B. M. Turner, Dosage compensation in mammals. *Cold Spring Harb. Perspect. Biol.* **7**, a019406 (2015).
8. S. H. Namekawa, B. Payer, K. D. Huynh, R. Jaenisch, J. T. Lee, Two-step imprinted X inactivation: Repeat versus genic silencing in the mouse. *Mol. Cell. Biol.* **30**, 3187–3205 (2010).
9. S. S. Tan, E. A. Williams, P. P. Tam, X-chromosome inactivation occurs at different times in different tissues of the post-implantation mouse embryo. *Nat. Genet.* **3**, 170–174 (1993).
10. M. Monk, M. I. Harper, Sequential X chromosome inactivation coupled with cellular differentiation in early mouse embryos. *Nature* **281**, 311–313 (1979).
11. E. G. Schulz *et al.*, The two active X chromosomes in female ESCs block exit from the pluripotent state by modulating the ESC signaling network. *Cell Stem Cell* **14**, 203–216 (2014).
12. G. F. Kay *et al.*, Expression of Xist during mouse development suggests a role in the initiation of X chromosome inactivation. *Cell* **72**, 171–182 (1993).
13. J. T. Lee, N. Lu, Targeted mutagenesis of Tsix leads to nonrandom X inactivation. *Cell* **99**, 47–57 (1999).
14. T. Sado, N. Brockdorff, Advances in understanding chromosome silencing by the long non-coding RNA Xist. *Philos. Trans. R. Soc. Lond. B Biol. Sci.* **368**, 20110325 (2013).
15. S. Sun *et al.*, Jpx RNA activates Xist by evicting CTCF. *Cell* **153**, 1537–1551 (2013).
16. Y. Ogawa, J. T. Lee, Xite, X-inactivation intergenic transcription elements that regulate the probability of choice. *Mol. Cell* **11**, 731–743 (2003).
17. C. Chureau *et al.*, Ftx is a non-coding RNA which affects Xist expression and chromatin structure within the X-inactivation center region. *Hum. Mol. Genet.* **20**, 705–718 (2011).
18. P. Navarro *et al.*, Molecular coupling of Xist regulation and pluripotency. *Science* **321**, 1693–1695 (2008).
19. P. Navarro *et al.*, Molecular coupling of Tsix regulation and pluripotency. *Nature* **468**, 457–460 (2010).
20. C. Gontan *et al.*, RNF12 initiates X-chromosome inactivation by targeting REX1 for degradation. *Nature* **485**, 386–390 (2012).
21. P. Navarro, M. Moffat, N. P. Mullin, I. Chambers, The X-inactivation trans-activator Rnf12 is negatively regulated by pluripotency factors in embryonic stem cells. *Hum. Genet.* **130**, 255–264 (2011).
22. B. M. Cattanach, J. H. Isaacson, Controlling elements in the mouse X chromosome. *Genetics* **57**, 331–346 (1967).
23. B. M. Cattanach, C. E. Williams, Evidence of non-random X chromosome activity in the mouse. *Genet. Res.* **19**, 229–240 (1972).
24. B. M. Cattanach, C. E. Pollard, J. N. Perez, Controlling elements in the mouse X-chromosome. I. Interaction with the X-linked genes. *Genet. Res.* **14**, 223–235 (1969).
25. J. D. West, V. M. Chapman, Variation for X chromosome expression in mice detected by electrophoresis of phosphoglycerate kinase. *Genet. Res.* **32**, 91–102 (1978).
26. P. G. Johnston, B. M. Cattanach, Controlling elements in the mouse. IV. Evidence of non-random X-inactivation. *Genet. Res.* **37**, 151–160 (1981).
27. B. M. Cattanach, C. Rasberry, Identification of the *Mus spretus* Xce allele. *Mouse Genome* **89**, 565–566 (1991).
28. E. de La Casa-Esperón *et al.*, X chromosome effect on maternal recombination and meiotic drive in the mouse. *Genetics* **161**, 1651–1659 (2002).
29. W. K. Krietsch, M. Fehlaup, P. Renner, T. Bücher, R. Fundele, Expression of X-linked phosphoglycerate kinase in early mouse embryos homozygous at the Xce locus. *Differentiation* **31**, 50–54 (1986).
30. B. M. Cattanach, J. N. Perez, Parental influence on X-autosome translocation-induced variegation in the mouse. *Genet. Res.* **15**, 43–53 (1970).
31. B. M. Cattanach, D. Papworth, Controlling elements in the mouse. V. Linkage tests with X-linked genes. *Genet. Res.* **38**, 57–70 (1981).
32. B. M. Cattanach, C. Rasberry, E. P. Evans, M. Burtenshaw, Further Xce linkage data. *Mouse News Lett.* **83**, 165 (1989).
33. M. C. Simmler, B. M. Cattanach, C. Rasberry, C. Rougeulle, P. Avner, Mapping the murine Xce locus with (CA)_n repeats. *Mamm. Genome* **4**, 523–530 (1993).
34. J. D. Calaway *et al.*, Genetic architecture of skewed X inactivation in the laboratory mouse. *PLoS Genet.* **9**, e1003853 (2013).
35. L. H. Chadwick, L. M. Pertz, K. W. Broman, M. S. Bartolomei, H. F. Willard, Genetic control of X chromosome inactivation in mice: Definition of the Xce candidate interval. *Genetics* **173**, 2103–2110 (2006).
36. A. T. Nguyen, Y. Zhang, The diverse functions of Dot1 and H3K79 methylation. *Genes Dev.* **25**, 1345–1358 (2011).
37. H. Niwa, J. Miyazaki, A. G. Smith, Quantitative expression of Oct-3/4 defines differentiation, dedifferentiation or self-renewal of ES cells. *Nat. Genet.* **24**, 372–376 (2000).
38. E. P. Nora *et al.*, Spatial partitioning of the regulatory landscape of the X-inactivation centre. *Nature* **485**, 381–385 (2012).
39. A. Minkovsky *et al.*, The pluripotency factor-bound intron 1 of Xist is dispensable for X chromosome inactivation and reactivation in vitro and in vivo. *Cell Rep.* **3**, 905–918 (2013).
40. M. Makhlof *et al.*, A prominent and conserved role for YY1 in Xist transcriptional activation. *Nat. Commun.* **5**, 4878 (2014).
41. J. D. Kim, C. Faulk, J. Kim, Retroposition and evolution of the DNA-binding motifs of YY1, YY2 and REX1. *Nucleic Acids Res.* **35**, 3442–3452 (2007).
42. D. E. Cohen *et al.*, The DXPas34 repeat regulates random and imprinted X inactivation. *Dev. Cell* **12**, 57–71 (2007).
43. M. F. Lyon, Possible mechanisms of X chromosome inactivation. *Nat. New Biol.* **232**, 229–232 (1971).
44. S. Rastan, Non-random X-chromosome inactivation in mouse X-autosome translocation embryos—Location of the inactivation centre. *J. Embryol. Exp. Morphol.* **78**, 1–22 (1983).
45. R. C. Spitale, M. C. Tsai, H. Y. Chang, RNA templating the epigenome: Long noncoding RNAs as molecular scaffolds. *Epigenetics* **6**, 539–543 (2011).
46. D. M. Ribeiro *et al.*, Protein complex scaffolding predicted as a prevalent function of long non-coding RNAs. *Nucleic Acids Res.* **46**, 917–928 (2018).
47. J. Dekker, E. Heard, Structural and functional diversity of topologically associating domains. *FEBS Lett.* **589**, 2877–2884 (2015).
48. R. Ghirlando, G. Felsenfeld, CTCF: Making the right connections. *Genes Dev.* **30**, 881–891 (2016).
49. R. Galupa *et al.*, A conserved noncoding locus regulates random monoallelic Xist expression across a topological boundary. *Mol. Cell* **77**, 352–367.e8 (2020).
50. A. A. Sigova *et al.*, Transcription factor trapping by RNA in gene regulatory elements. *Science* **350**, 978–981 (2015).
51. F. A. Ran *et al.*, Genome engineering using the CRISPR-Cas9 system. *Nat. Protoc.* **8**, 2281–2308 (2013).
52. Q. L. Ying *et al.*, The ground state of embryonic stem cell self-renewal. *Nature* **453**, 519–523 (2008).
53. M. Attia, C. Rachez, P. Avner, U. C. Rogner, Nucleosome assembly proteins and their interacting proteins in neuronal differentiation. *Arch. Biochem. Biophys.* **534**, 20–26 (2013).
54. J. Chaumeil, I. Okamoto, E. Heard, X-chromosome inactivation in mouse embryonic stem cells: Analysis of histone modifications and transcriptional activity using immunofluorescence and FISH. *Methods Enzymol.* **376**, 405–419 (2004).
55. S. H. Namekawa, J. T. Lee, Detection of nascent RNA, single-copy DNA and protein localization by immunofluorescence in mouse germ cells and preimplantation embryos. *Nat. Protoc.* **6**, 270–284 (2011).
56. A. Dubois *et al.*, Spontaneous reactivation of clusters of X-linked genes is associated with the plasticity of X-inactivation in mouse trophoblast stem cells. *Stem Cells* **32**, 377–390 (2014).